ELSEVIER

Applied Mathematical Modelling 22 (1998) 703–725

APPLIED MATHEMATICAL MODELLING

Analytical study and numerical experiments for Laplace equation with overspecified boundary conditions

J.T. Chen *, K.H. Chen

Department of Harbor and River Engineering, National Taiwan Ocean University, P.O. Box 7-59, Keelung, Taiwan ROC

Received 19 June 1997; accepted 2 June 1998

Abstract

In this paper, the window function, $e^{-\alpha k^2}$, is applied to regularize the divergent problem which occurs in the Laplace equation with overspecified boundary conditions in an infinite strip region. To deal with this ill-posed problem, the corner of the L-curve is chosen as the compromise point to determine the optimal α of the Gaussian window, $e^{-\alpha k^2}$, so that the high wave-number (k) content can be suppressed instead of engineering judgement using the concept of a cutoff wave-number. From the examples shown, it is found that a reasonable solution of the unknown boundary potential can be reconstructed, and that both high wave-number content and divergent results can be avoided by using the proposed regularization technique.

1. Introduction

Inverse problems are presently becoming more important in many fields of science and engineering [1,2]. The Laplace equation of an infinite strip with overspecified boundary conditions (B.C.s) can be treated as an inverse problem [3]. Sometimes, unreasonable results occur in the inverse analysis due to the measured and contaminated errors or the limited accuracy of the computer in the input B.C. [4]. Mathematically speaking, the inverse problem is ill-posed since the solution is very sensitive to the given data. This phenomenon will become more serious when the depth of the strip is greater. This paper focuses on a treatment for divergence of solution due to noise on the overspecified B.C.s. The depth of the strip is assumed to be known. Such a divergent problem could be avoided by using a cutoff wave-number or regularization methods. The former method utilizes a rectangular window to eliminate all the high wave-number contents which are larger than the cutoff wave-number as used in SHAKE program [5]. Nevertheless, how a suitable cutoff wave-number is chosen depends on engineering judgement in engineering practice. For example, Silva suggested a cutoff frequency of 15 Hz to eliminate the tendency to develop unrealistically large accelerations at depth [6]. Nevertheless, the side lobe of the rectangular window is large. To find an optimum window with a general rule is a key step in solving such a problem. The regularization techniques have been successfully applied to solve direct and inverse problems.

* Corresponding author. Fax: +886 2 462 2192/6102; e-mail: bo209@ntou66.ntou.edu.tw.

0307-904X/98/$ – see front matter
PII: S0307-904X(98)10054-9

For example, three regularization techniques, Cesàro sum, quasi-static decomposition and Stokes' transformation, have been applied to direct problems by Chen and Hong [7–13] when the analytical solution is not expressed in the best way. The three methods can obtain the solution more precisely. One of the regularization techniques, the Cesàro window, has been successfully applied to deconvolution analysis of site response in earthquake engineering by Chen et al. [4] in conjunction with the L-curve concept.

In this paper, we shall employ one of the regularization methods, the window function, $e^{-\alpha k^2}$ [3], to circumvent the ill-posed problem. In other words, an optimum Gaussian window, $e^{-\alpha k^2}$, with an appropriate α, will be introduced. The window function, $e^{-\alpha k^2}$, can redistribute the amplitude of the wave-number content for the system kernel; therefore, an ill-posed problem can be transformed into a well-posed one by choosing an appropriate number for α. The appropriate number is determined according to a compromise between regularization errors (due to data smoothing) and perturbation errors (due to noise disturbance) [14]. The corner of the L-curve determines the optimal value of α which will be employed to provide the compromise point and will be elaborated on later. Also, comparison of the ill-posed problem for the wave equation, Laplace equation and heat conduction equation with overspecified B.C.s will be discussed. The index of ill-posedness for the Laplace equation is larger than that for the other two because its transfer function diverges more seriously as the wave-number becomes large. Therefore, the inverse problem of the Laplace equation will diverge more seriously. This is the reason why we treat the Laplace equation in this paper. Finally, examples contaminated with artificial noises for both direct and inverse problems will be shown to illustrate the validity of the proposed technique.

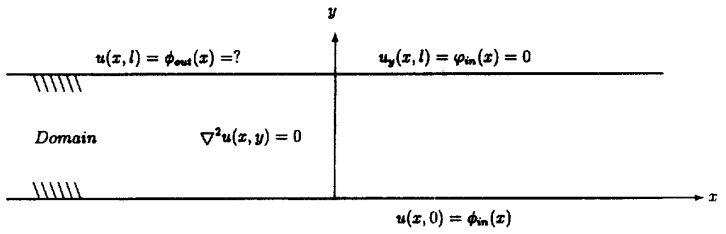

(a) Model 1

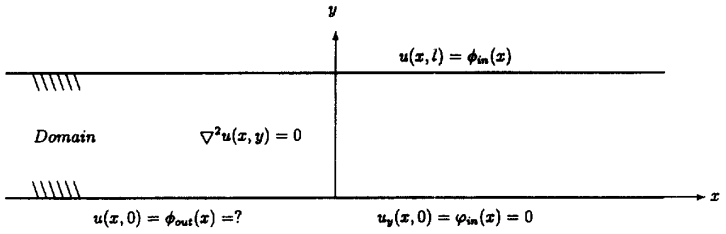

(b) Model 2

Fig. 1. Direct problems for the Laplace equation in an infinite strip.

2. Formulation of the Laplace equation with over-specified boundary conditions

In general, the direct and inverse problems for the Laplace equation of an infinite strip can be illustrated as shown in Figs. 1 and 2, respectively. For the direct problems, in Fig. 1(a) and (b), the known boundary potential $\phi_{in}(x)$ and boundary flux $\varphi_{in}(x)$ in the space domain (x domain) or $\Phi_{in}(k)$ and $\Psi_{in}(k)$ in the wave-number domain (k domain) are prescribed over different boundaries ($y = 0, y = l$), respectively. For inverse problems, in Fig. 2(a) and (b), the known boundary potential $\phi_{in}(x)$ and boundary flux $\varphi_{in}(x)$ in the x domain or $\Phi_{in}(k)$ and $\Psi_{in}(k)$ in the k domain are overspecified on the same boundary ($y = 0, y = l$), but the flux and potential on the remaining boundary are both unknown.

By using the Fourier transform, we can construct the analytical solution for the Laplace equation in terms of integral form as follows.

(1) Direct problem: From Fig. 1(a), the unknown potential solution can be represented as

$$u(x,y) = \frac{1}{2\pi}\int_{-\infty}^{\infty}\left[T_{d_1}^{\phi}(k,y)\Phi_{in}(k) + T_{d_1}^{\varphi}(k,y)\Psi_{in}(k)\right]e^{ikx}\,dk, \tag{1}$$

where $\Phi_{in}(k)$ and $\Psi_{in}(k)$ are the known boundary potential ($y = 0$) and boundary flux ($y = l$) in the k domain, k is the wave-number, $T_{d_1}^{\phi}(k,y)$ and $T_{d_1}^{\varphi}(k,y)$ are the transfer functions of direct problems in the k domain, as expressed by

$$T_{d_1}^{\phi}(k,y) = \frac{\cosh k(y-l)}{\cosh(kl)}, \tag{2}$$

$$T_{d_1}^{\varphi}(k,y) = \frac{\sinh(ky)}{k\cosh(kl)}, \tag{3}$$

in which l is the thickness of the strip. Therefore, the unknown potential on the boundary ($y = l$) is

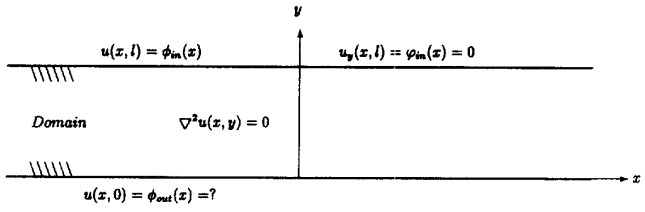

(a) Model 1

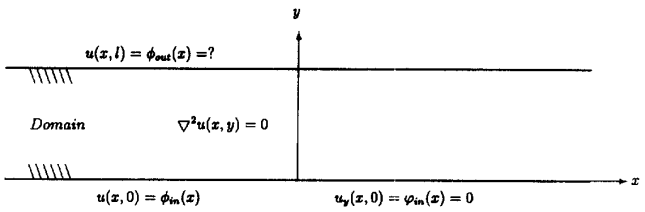

(b) Model 2

Fig. 2. Inverse problems for the Laplace equation in an infinite strip.

$$u(x,l)=\phi_{\text{out}}(x)=\frac{1}{2\pi}\int_{-\infty}^{\infty}\left[\frac{1}{\cosh(kl)}\Phi_{\text{in}}(k)+\frac{\sinh(kl)}{k\cosh(kl)}\Psi_{\text{in}}(k)\right]e^{ikx}\,dk, \tag{4}$$

where $\phi_{\text{out}}(x)$ is the unknown boundary potential ($y=l$).

From Fig. 1(b), the unknown potential ($y=0$) can be represented as

$$u(x,y)=\frac{1}{2\pi}\int_{-\infty}^{\infty}\left[T_{d_2}^{\phi}(k,y)\Phi_{\text{in}}(k)+T_{d_2}^{\varphi}(k,y)\Psi_{\text{in}}(k)\right]e^{ikx}\,dk, \tag{5}$$

where $T_{d_2}^{\phi}(k,y)$ and $T_{d_2}^{\varphi}(k,y)$ are the transfer functions of direct problems in the k domain as expressed by

$$T_{d_2}^{\phi}(k,y)=\frac{\cosh(ky)}{\cosh(kl)}, \tag{6}$$

$$T_{d_2}^{\varphi}(k,y)=\frac{\sinh k(y-l)}{k\cosh(kl)}. \tag{7}$$

Therefore, the unknown potential on the boundary ($y=0$) is

$$u(x,0)=\phi_{\text{out}}(x)=\frac{1}{2\pi}\int_{-\infty}^{\infty}\left[\frac{1}{\cosh(kl)}\Phi_{\text{in}}(k)+\frac{\sinh(-kl)}{k\cosh(kl)}\Psi_{\text{in}}(k)\right]e^{ikx}\,dk. \tag{8}$$

It is found that the transfer functions in Eqs. (2), (3), (6) and (7) for direct problems are bounded as k grows to infinity.

(2) Inverse problem: From Fig. 2(a), the unknown potential ($y=0$) can be represented as

$$u(x,y)=\frac{1}{2\pi}\int_{-\infty}^{\infty}\left[T_{i_1}^{\phi}(k,y)\Phi_{\text{in}}(k)+T_{i_1}^{\varphi}(k,y)\Psi_{\text{in}}(k)\right]e^{ikx}\,dk, \tag{9}$$

where $T_{i_1}^{\phi}(k,y)$ and $T_{i_1}^{\varphi}(k,y)$ are the transfer functions in the k domain for inverse problems as expressed by

$$T_{i_1}^{\phi}(k,y)=\cosh k(y-l), \tag{10}$$

$$T_{i_1}^{\varphi}(k,y)=\frac{\sinh k(y-l)}{k}. \tag{11}$$

Therefore, the unknown potential on the boundary ($y=0$) is

$$u(x,0)=\phi_{\text{out}}(x)=\frac{1}{2\pi}\int_{-\infty}^{\infty}\left[\cosh(kl)\Phi_{\text{in}}(k)+\frac{\sinh(-kl)}{k}\Psi_{\text{in}}(k)\right]e^{ikx}\,dk. \tag{12}$$

From Fig. 2(b), the unknown potential ($y=l$) can be represented as

$$u(x,y)=\frac{1}{2\pi}\int_{-\infty}^{\infty}\left[T_{i_2}^{\phi}(k,y)\Phi_{\text{in}}(k)+T_{i_2}^{\varphi}(k,y)\Psi_{\text{in}}(k)\right]e^{ikx}\,dk, \tag{13}$$

where $T_{i_2}^{\phi}(k,y)$ and $T_{i_2}^{\varphi}(k,y)$ are transfer functions in the k domain for inverse problems and can be expressed as

$$T_{i_2}^{\phi}(k,y)=\cosh(ky), \tag{14}$$

$$T^{\varphi}_{i_2}(k,y) = \frac{\sinh(ky)}{k}. \tag{15}$$

Therefore, the unknown potential on the boundary, $y = l$, is

$$u(x,l) = \phi_{\text{out}}(x) = \frac{1}{2\pi}\int_{-\infty}^{\infty}\left[\cosh(kl)\Phi_{\text{in}}(k) + \frac{\sinh(kl)}{k}\Psi_{\text{in}}(k)\right]e^{ikx}\,dk. \tag{16}$$

It is found that the transfer functions in Eqs. (10), (11), (14) and (15) for the inverse problems are unbounded as k grows to infinity.

In the above direct and inverse problems, eight transfer functions have been obtained. The explicit forms are summarized below:

$$T^{\phi}_{d_1}(k,y) = \frac{\cosh\ k(y-l)}{\cosh\ kl}, \tag{17}$$

$$T^{\varphi}_{d_1}(k,y) = \frac{\sinh\ ky}{k\ \cosh\ kl}, \tag{18}$$

$$T^{\phi}_{d_2}(k,y) = \frac{\cosh\ ky}{\cosh\ kl}, \tag{19}$$

$$T^{\varphi}_{d_2}(k,y) = \frac{\sinh\ k(y-l)}{k\ \cosh\ kl}, \tag{20}$$

$$T^{\phi}_{i_1}(k,y) = \cosh\ k(y-l), \tag{21}$$

$$T^{\phi}_{i_1}(k,y) = \frac{\sinh\ k(y-l)}{k}, \tag{22}$$

$$T^{\varphi}_{i_2}(k,y) = \cosh\ ky, \tag{23}$$

$$T^{\varphi}_{i_2}(k,y) = \frac{\sinh\ ky}{k}. \tag{24}$$

From Eqs. (17) and (21), we have

$$T^{\phi}_{d_1}(k,l)T^{\phi}_{i_1}(k,0) = 1. \tag{25}$$

From Eqs. (18) and (22), we have

$$\frac{\partial T^{\varphi}_{d_1}(k,0)}{\partial y}\frac{\partial T^{\varphi}_{i_1}(k,0)}{\partial y} = 1. \tag{26}$$

From Eqs. (19) and (23), we have

$$H^{\phi}_{d_2}(k,0)T^{\phi}_{i_2}(k,l) = 1. \tag{27}$$

From Eqs. (20) and (24), we have

$$\frac{\partial T^{\varphi}_{d_2}(k,l)}{\partial y}\frac{\partial T^{\varphi}_{i_2}(k,l)}{\partial y} = 1. \tag{28}$$

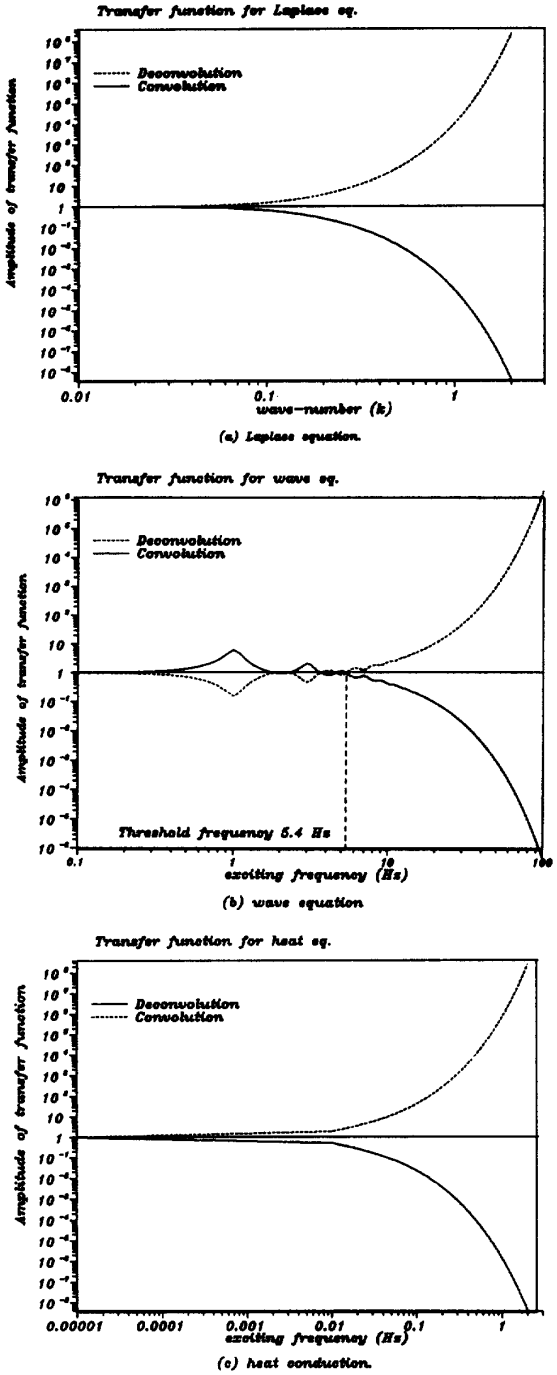

Fig. 3. Transfer functions of convolution and deconvolution for the Laplace equation, wave equation and heat conduction.

Eqs. (25)–(28) reveal that transfer functions for direct and inverse problems are inverse to each other. For simplicity, if the potential flux, $\varphi_{\text{in}}(x)$, is zero, then the solution of direct problems can be reduced to

$$\phi_{\text{out}}(x) = \frac{1}{2\pi}\int_{-\infty}^{\infty} T_d(k)\Phi_{\text{in}}(k)e^{ikx}\,dk, \tag{29}$$

where $T_d(k) = 1/\cosh(kl)$, and the unknown boundary potential in the k domain for the direct problem can be represented as

$$\Phi_{\text{out}}(k) = T_d(k)\Phi_{\text{in}}(k), \tag{30}$$

in which

$$T_d(k) = T_{d_1}^{\phi}(k,l) = T_{d_2}^{\phi}(k,0) = \frac{1}{\cosh(kl)}. \tag{31}$$

When the known potential $\Phi_{\text{in}}(k)$ in one boundary is given, and the known flux $\Psi_{\text{in}}(k)$ in the remaining boundary is zero, the unknown potential $\Phi_{\text{out}}(k)$ can be calculated according to

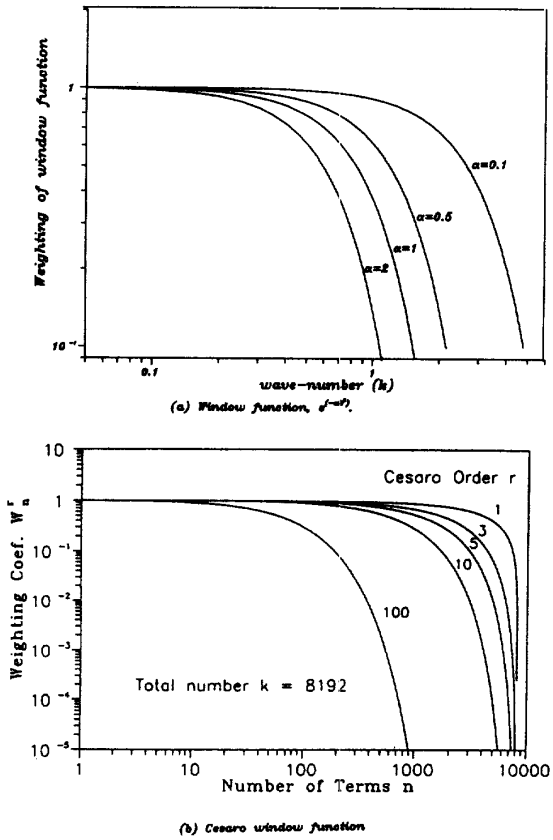

Fig. 4. Gaussian window function and Cesàro window function.

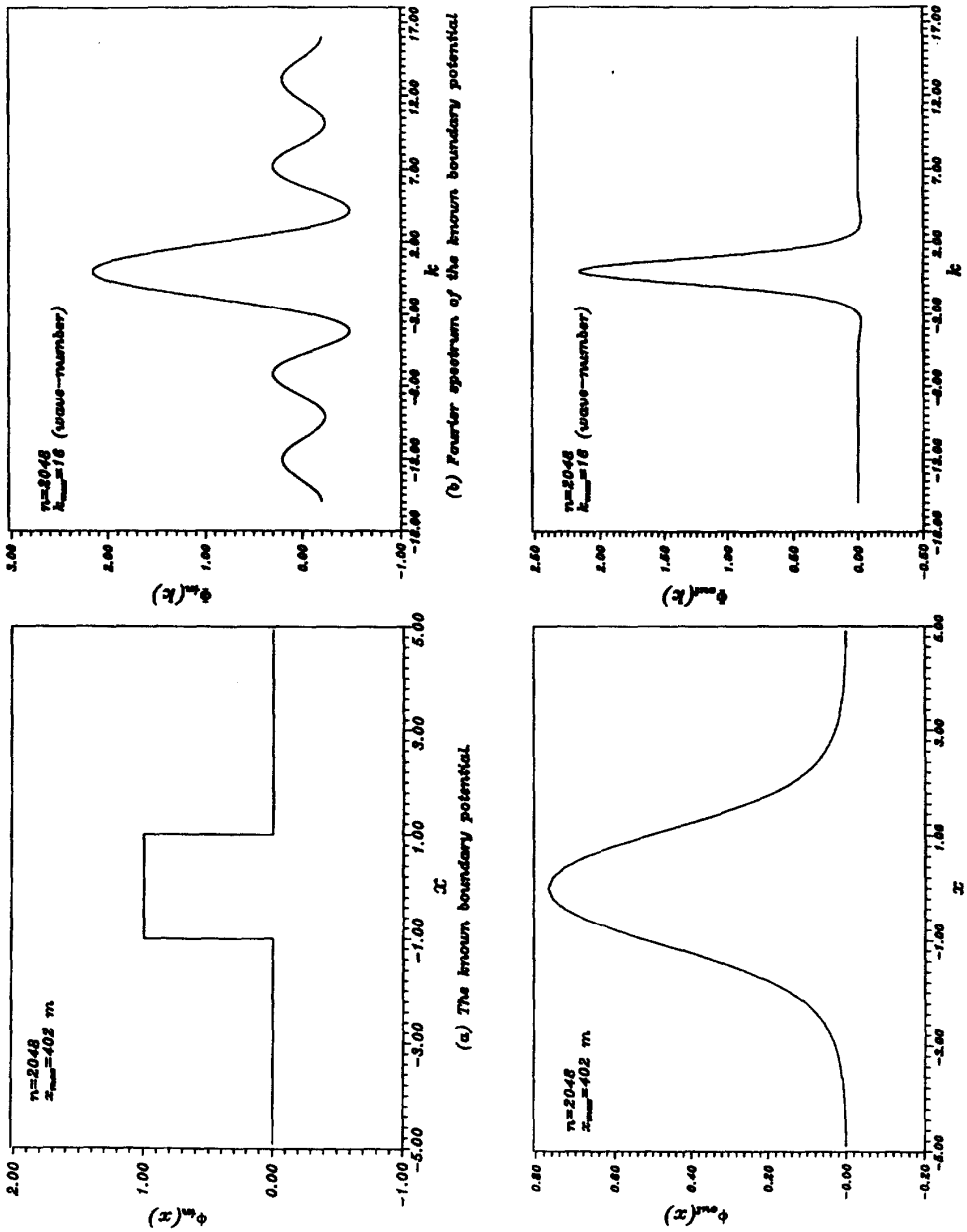

Fig. 5. The known and unknown boundary potentials and their Fourier spectra in the convolution analysis for case 1.

Eq. (30). This procedure is usually called the "direct process," and $T_d(k)$ is the transfer function of convolution for the Laplace equation. On the other hand, the transfer function for the inverse problem can be defined as

$$T_i(k) = \frac{\Phi_{\text{out}}(k)}{\Phi_{\text{in}}(k)} = \cosh(kl). \tag{32}$$

When $\Phi_{\text{in}}(k)$ is given in one boundary, and $\Psi_{\text{in}}(k)$ is zero in the same boundary, $\Phi_{\text{out}}(k)$ can be represented as

$$\Phi_{\text{out}}(k) = T_i(k)\Phi_{\text{in}}(k) \tag{33}$$

$$= \cosh(kl)\Phi_{\text{in}}(k). \tag{34}$$

Eq. (33) can be called the "inverse process," and $\phi_{\text{out}}(x)$ can be obtained by inverse discrete Fourier transform as represented by

$$\phi_{\text{out}}(x) = \sum_{n=-\infty}^{\infty} \Phi_{\text{out}}(k_n)\mathrm{e}^{\mathrm{i}k_n x}, \tag{35}$$

where k_n is nth wave-number in the Fourier domain. In practical calculations, only the finite length of the summation is used; therefore, Eq. (35) is changed to

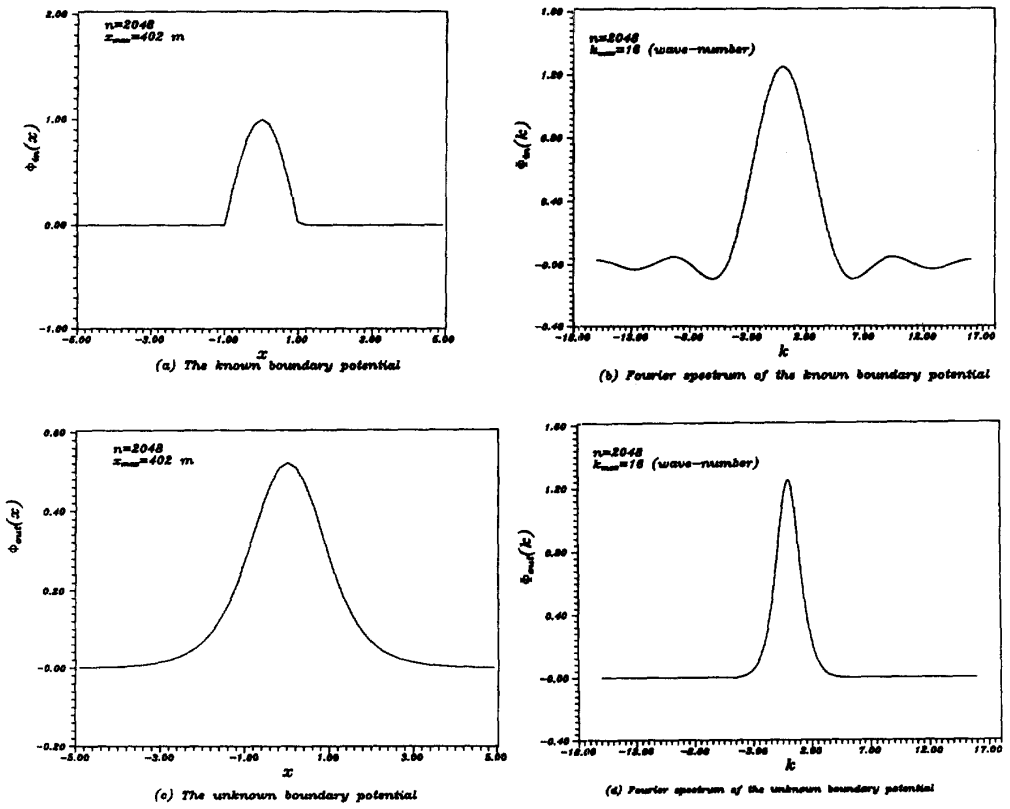

Fig. 6. The known and unknown boundary potentials and their Fourier spectra in the convolution analysis for case 2.

$$\phi_{\text{out}}(x) = \sum_{n=-N}^{N} \Phi_{\text{out}}(k_n) e^{ik_n x}, \tag{36}$$

where N is total number in the discrete Fourier transform.

Comparing Eq. (31) with Eq. (32), it can be seen that $T_d(k)$ is the inverse of $T_i(k)$. A typical relationship of their amplitude versus wave-number is shown in Fig. 3(a). The amplitude of the transfer function for the direct problem decreases rapidly as the wave-number increases. On the other hand, the amplitude of the transfer function for the inverse problem becomes larger as the wave-number becomes higher. Comparing with the wave equation [4] and heat conduction, as shown in Fig. 3(b) and (c), we can find the same trend. Since the transfer function of the convolution analysis is bounded, no serious errors will occur when the input data is contaminated with noise. However, the transfer function for the inverse problem has very high amplitude in the range where the wave-number is larger. This means that the transfer function can amplify any high wave-number noise of the contaminated input data in the deconvolution analysis.

In engineering practice, records (including the boundary potential and boundary flux) on a boundary may not be available. Therefore, deconvolution analysis must be used to calculate the

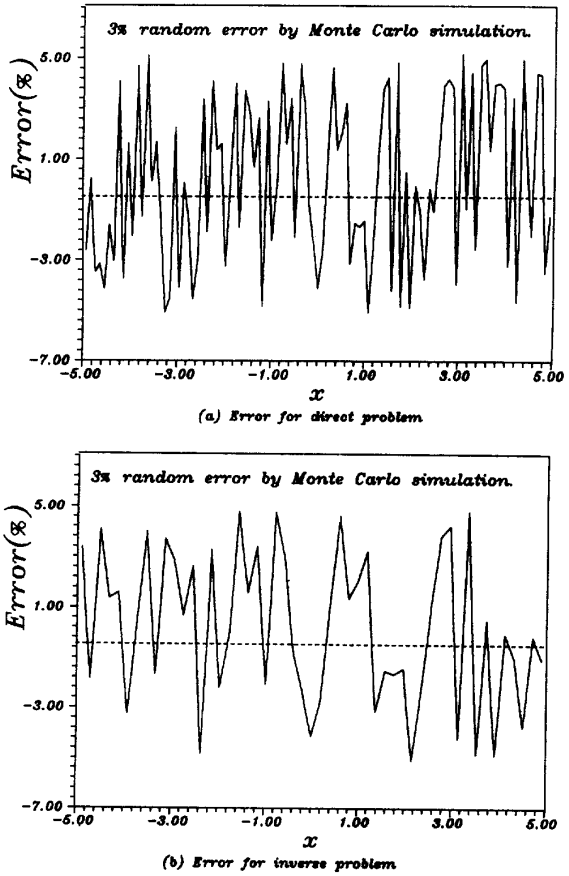

Fig. 7. The random errors in the convolution and deconvolution analysis.

potential on the boundary where it is not easy to measure. The problem of high wave-number amplification can not be avoided in the analysis. Therefore, noise errors should be suppressed by using a regularization technique. Section 3 will introduce a regularization method to overcome the difficulty of high wave-number amplification in the deconvolution analysis.

3. Regularization technique with Gaussian window

For the above mentioned ill-posed problem, regularization techniques are often employed to transform the original problem into a well-posed one. The problem will be dealt with in the k domain. Therefore, we will propose a regularization technique based on the window function, $e^{-\alpha k^2}$, to regularize the ill-posed problem in the k domain. In the mathematical modelling for a physical problem, the series representation or integral representation for the solution is often assumed, and the governing equation in another domain can be equivalently obtained. In order to represent the solution more accurately when the input data has some noise errors, a regularization technique can be used to reproduce the unknown solution more precisely. This is the reason why the window function, $e^{-\alpha k^2}$, is related to the reproducing kernel and Cesàro window [4].

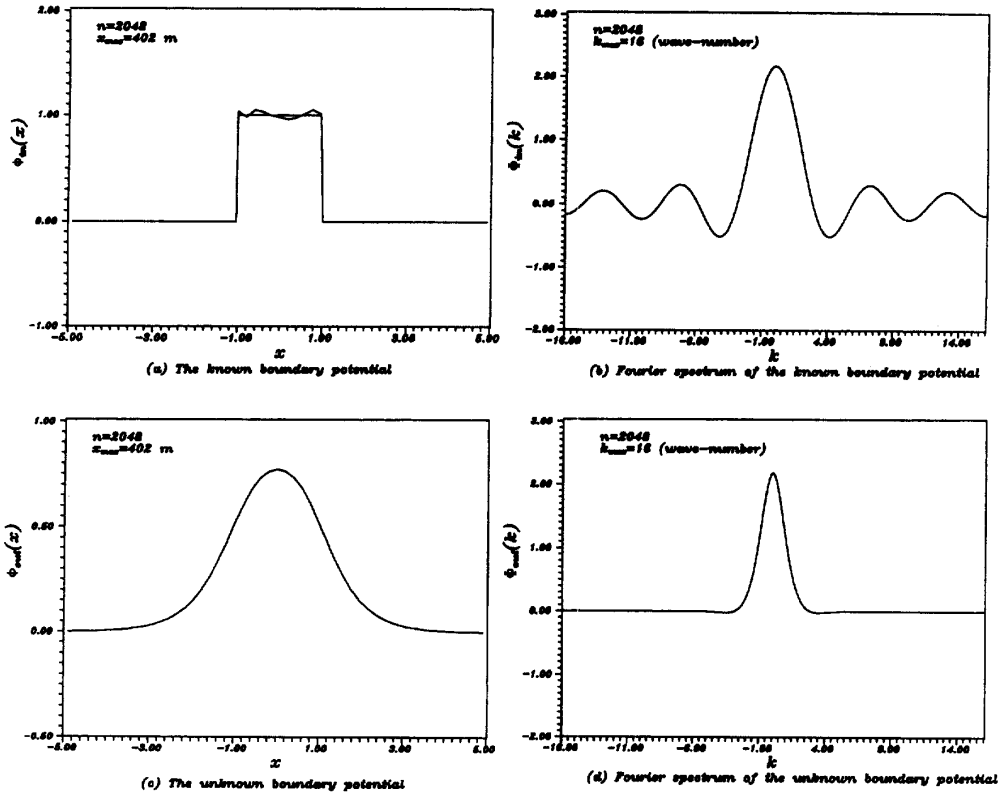

Fig. 8. The contaminated known and unknown boundary potentials and their Fourier spectra in the convolution analysis for case 1.

The Gaussian window, $e^{-\alpha k^2}$, can be represented as a weight function which can suppress the amplitude of a high wave-number. To understand the effect of the weights for different values of α (0.1,0.5,1,2), their values are shown in Fig. 4(a). It is interesting to find the same trend as we find with the Cesàro orders 1, 5, 10, 20, 100 as shown in Fig. 4(b) [4]. It is seen that the window function $e^{-\alpha k^2}$, and the Cesàro mean have the same physical meaning as a window function. The larger α is, the more seriously the high wave-number content will be suppressed. Therefore, if the window function is applied to deconvolution analysis in the k domain, the amplitude of the high wave-number content can be suppressed, and the solution will be insensitive to high-wave number input errors. Applying the window function, $e^{-\alpha k^2}$, to the deconvolution analysis, Eq. (36) can be replaced by

$$\phi^{\alpha}_{\text{out}}(x) = \sum_{n=-N}^{n=N} e^{-\alpha k_n^2} \Phi_{\text{out}}(k_n) e^{ik_n x}, \tag{37}$$

where $\phi^{\alpha}_{\text{out}}(x)$ is a regularized solution instead of the unregularized solution $\phi_{\text{out}}(x)$ in Eq. (36). The inverse Fourier transform of the window function, $e^{-\alpha k^2}$, is

$$W_{\alpha}(x) = \frac{1}{2\sqrt{\alpha\pi}} e^{-x^2/4\alpha}. \tag{38}$$

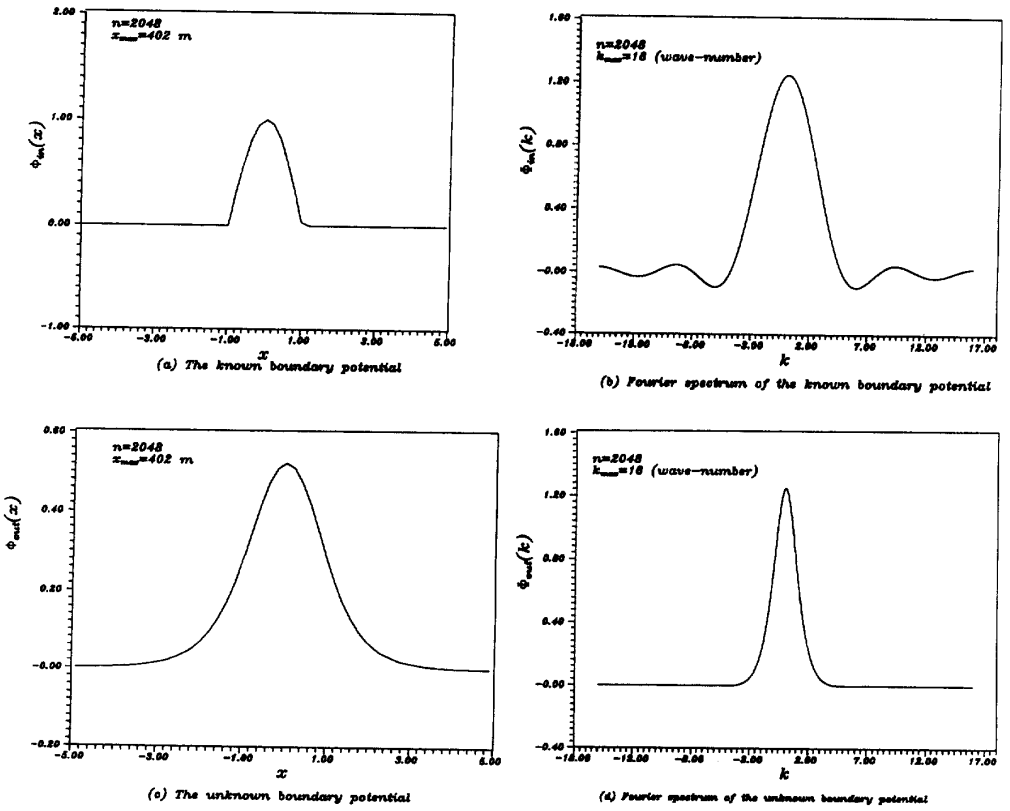

Fig. 9. The contaminated known and unknown boundary potentials and their Fourier spectra in the convolution analysis for case 2.

By using the convolution product, the regularized solution can be represented as

$$\phi^{\alpha}_{\text{out}}(x) = \int_{-\infty}^{\infty} W_{\alpha}(x-\tau)\phi_{\text{out}}(\tau)\,\mathrm{d}\tau, \tag{39}$$

where $W_{\alpha}(x-\tau)$ is a reproducing kernel, and

$$|\phi^{\alpha}_{\text{out}}(x) - \phi_{\text{out}}(x)| = \left|c\sqrt{\alpha}\left(\frac{1}{\pi}+1\right)\right|, \tag{40}$$

in which c is a constant larger than zero, and

$$\lim_{\alpha\to 0}\phi^{\alpha}_{\text{out}}(x) = \phi_{\text{out}}(x). \tag{41}$$

This is the reason why we choose the Gaussian window [3].

4. The L-curve and its applications

Most numerical methods for treating ill-posed problems seek to overcome problems associated with an ill-conditioned system by replacing the problem with a "nearby" well-conditioned

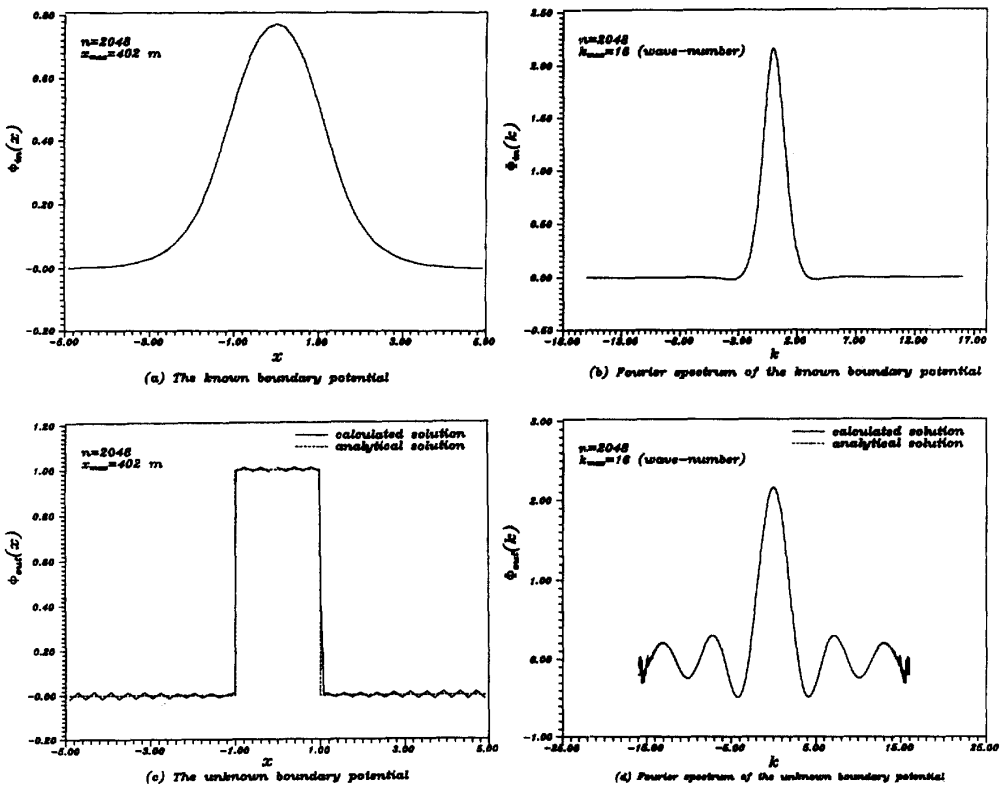

Fig. 10. The known and unknown boundary potentials and their Fourier spectra in the deconvolution analysis for case 1.

problem, whose solution approximates the required solution and, in addition, is a more satisfactory solution than is the ordinary solution. The latter goal is achieved by incorporating additional information about the sought after solution, and often the computed solution should be smooth. Such methods are called regularization methods, and they always include a so called regularization parameter, which controls the degree of smoothing. Now, the α of the window function, $e^{-\alpha k^2}$, is chosen as the parameter of smoothness. A very convenient way of displaying the judgement of the optimal parameter is the L-curve, which was first presented by Hanson [14]. In the L-curve concept, the x-axis is the solution norm, and the y-axis is the residual norm. The former is the index of how smoothly the solution is treated, and the latter is the distance index between the predicted output and the real output. In deconvolution analysis, after obtaining the unknown boundary potential in the inverse problem, we can transform the problem into a direct problem by using the known B.C. By using the convolution process for the direct problem, we can obtain a new potential which has been known on this boundary. By comparing the new potential with the known boundary potential, the difference norm can be seen as the y-axis, and the value of α is the x-axis. In this way, we can easily get a compromise between the regularization errors due to data smoothing and perturbation errors in measurements or other noise, even though an analytical solution is not available. According to the L-curve concept, the corner region is the appropriate choice for the regularization parameter, i.e., the α of the Gaussian window, $e^{-\alpha k^2}$.

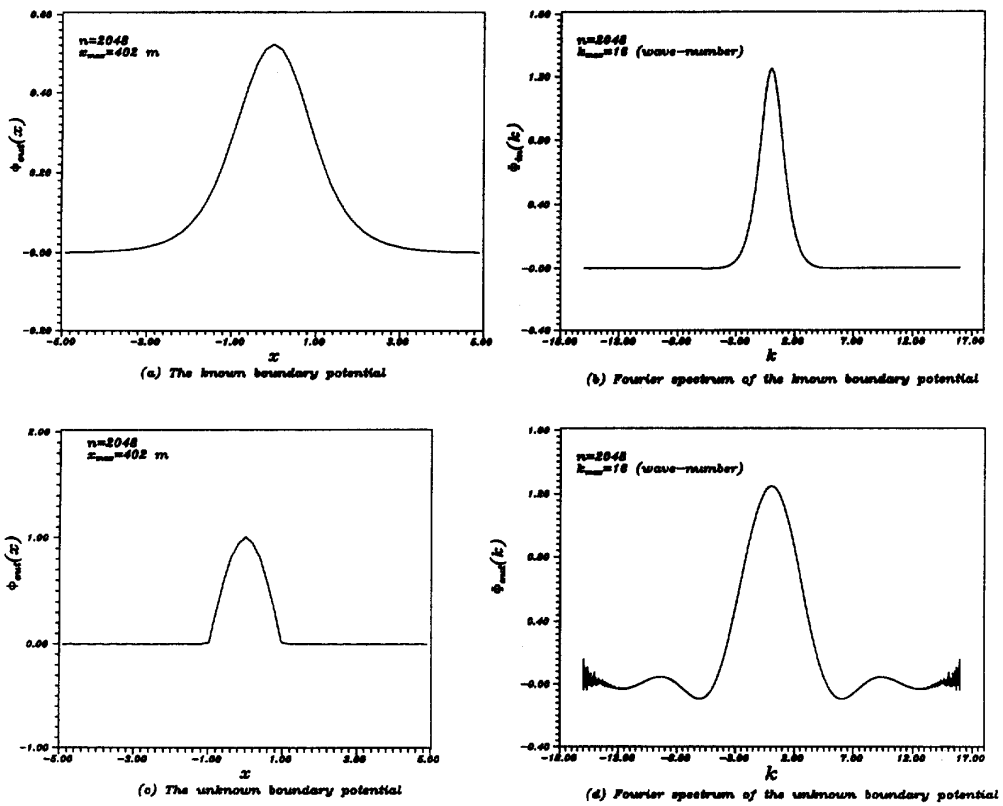

Fig. 11. The known and unknown boundary potentials and their Fourier spectra in the deconvolution analysis for case 2.

5. Numerical examples, results and discussion

To illustrate application of the $e^{-\alpha k^2}$ window and the L-curve for the Laplace equation with overspecified B.C.s, an infinite strip with finite thickness, $l = 1$, is chosen as a representation example. Two kinds of problems are considered: one is the direct problem with and without noise, and the other is the inverse problem with and without noise.

(1) *Direct problem: convolution analysis.* The present model of the direct problem can be described as shown in Fig. 1(a). Suppose two functions are given in the known boundary potentials ($y = 0$) of the two cases, $\phi_{in}(x)$, as shown in Figs. 5(a) and 6(a), and suppose the known boundary fluxes of the two cases, $\varphi_{in}(x)$, on the other boundary ($y = l$) are zero. Their Fourier amplitudes, $\Phi_{in}(k)$, are shown in Figs. 5(b) and 6(b). By the direct process, the unknown boundary potentials of the two cases, $\phi_{out}(x)$, and their Fourier spectrums, $\Phi_{out}(k)$, can be obtained by Eq. (30) as shown in Figs. 5(c), (d) and 6(c), (d). Comparing Fig. 5(b) with Figs. 5(d) and 6(b) with Fig. 6(d), it can be found that the unknown boundary potentials of the two cases, $\Phi_{out}(k)$, have less high wave-number content as compared with the known boundary potentials of the two cases, $\Phi_{in}(k)$. By using Monte Carlo simulation, we can obtain 3% random errors contaminating the input data, as shown in Fig. 7(a). The known boundary potentials of the two cases, $\phi_{in}(x)$, are

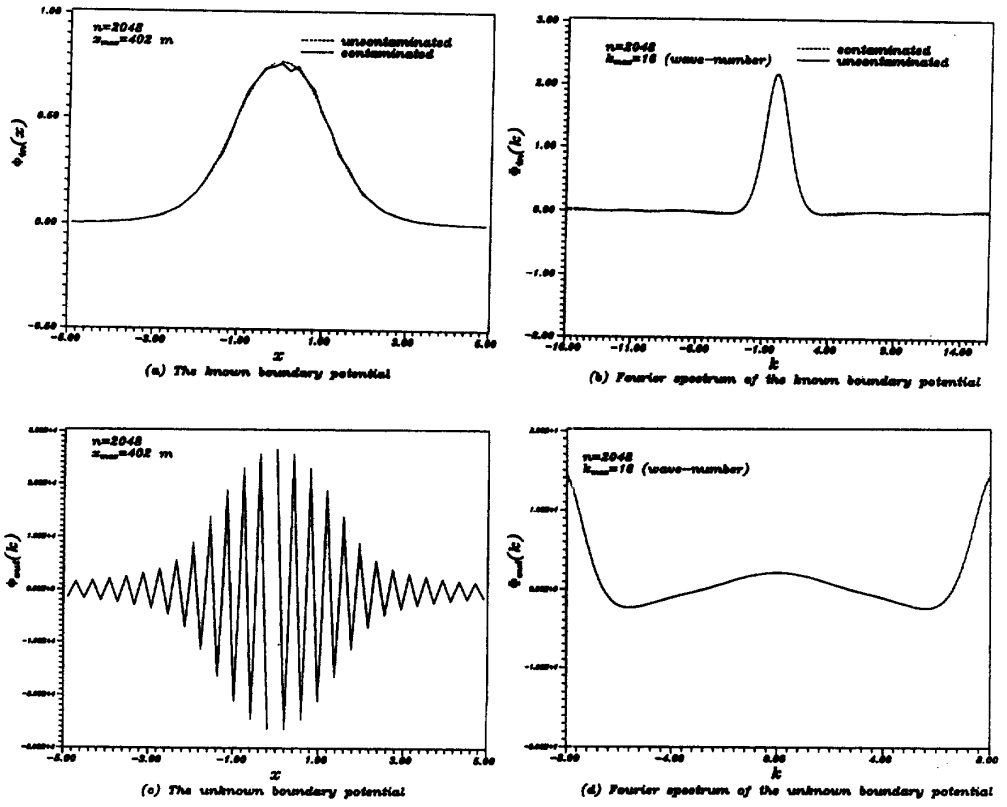

Fig. 12. The contaminated known and unknown boundary potentials and their Fourier spectra in the deconvolution analysis for case 1.

contaminated by the noise errors to simulate probable errors in the measurement. The contaminated potentials and their Fourier spectra on the known boundary for the two cases are shown in Fig. 8(a), (b) and Fig. 9(a), (b). The results using the direct process are shown in Fig. 8(c), (d) and Fig. 9(c), (d), and no significant difference can be found. Therefore, the regularization technique is not necessary for the direct problem even though the data is contaminated with errors.

(2) *Inverse problem: deconvolution analysis.* The present model of the inverse problem can be described as shown in Fig. 2(a). The unknown boundary potentials ($y = l$), $\phi_{\text{out}}(x)$, for the two cases in the convolution analysis are seen as the known boundary conditions of potentials for the two cases, $\phi_{\text{in}}(x)$, in the deconvolution analysis, as shown in Fig. 10(a), (b) and Fig. 11(a), (b). The known fluxes of the two cases, $\varphi_{\text{in}}(x)$, for the two cases on the same boundary ($y = l$) are zero. By using the inverse process, we obtain the unknown boundary potentials, $\phi_{\text{out}}(x)$, as shown in Fig. 10(c), (d) and Fig. 11(c), (d). The results are satisfactory as compared with the analytical solution. To see the influence of high wave-number noise in the deconvolution analysis, we can obtain 3% random errors, shown in Fig. 7(b), and superimpose them to simulate probable errors in measurement. The contaminated potentials and their Fourier spectra on the overspecified boundary for the two cases are shown in Fig. 12(a), (b) and Fig. 13(a), (b). It is found that, if

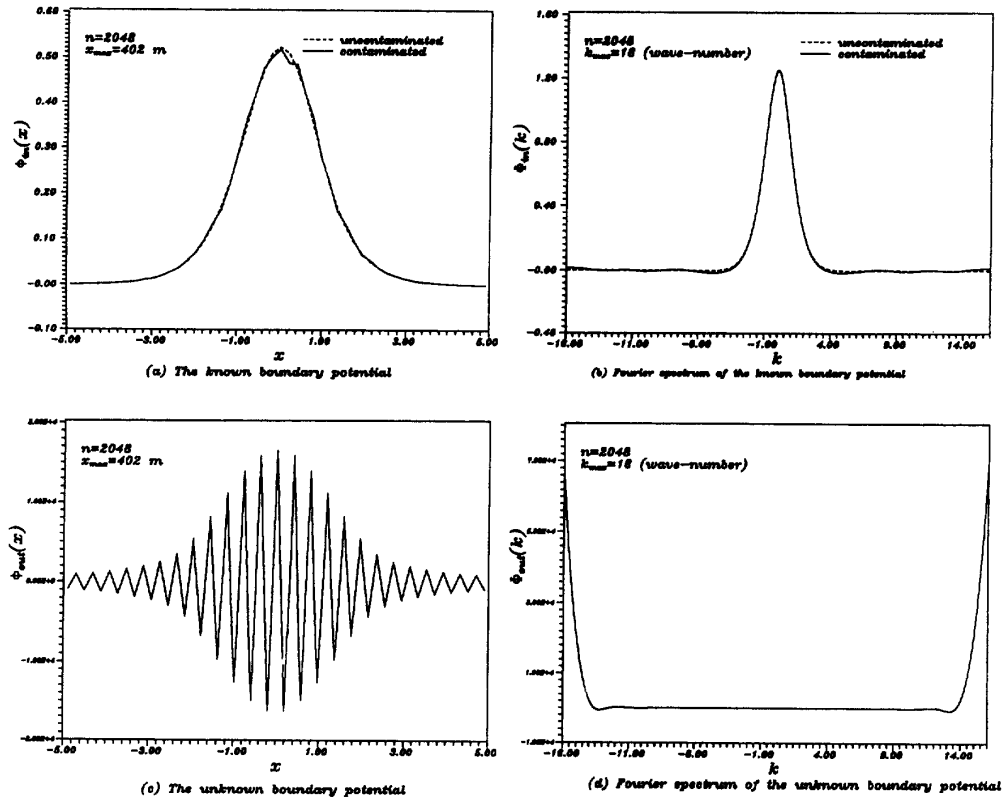

Fig. 13. The contaminated known and unknown boundary potentials and their Fourier spectra in the deconvolution analysis for case 2.

regularization technique is not employed, the results are unreasonable as shown in Figs. 12(c), (d) and 13(c), (d). In the inverse process, too much high wave-number content is present, and the solution is unrealistic and divergent.

When the Gaussian window, $e^{-\alpha k^2}$, is applied in the deconvolution analysis for the two cases, we can obtain solutions with many values of α, as shown in Fig. 14(a), (b) and Fig. 15(a), (b). Therefore, we can find the relationship between the residual norm and the value of α; i.e., the L-curve, as shown in Figs. 16 and 17, can be constructed. As expected from the mathematical point of view, a corner is present in the L-curve. When the value of α is at the left hand side of

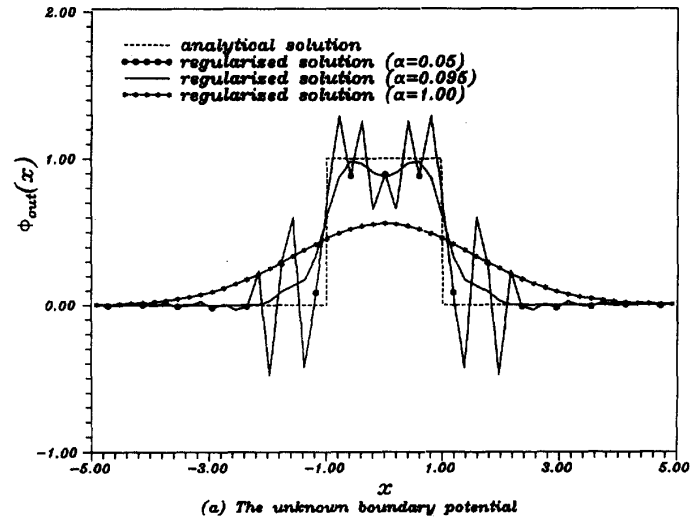

(a) The unknown boundary potential

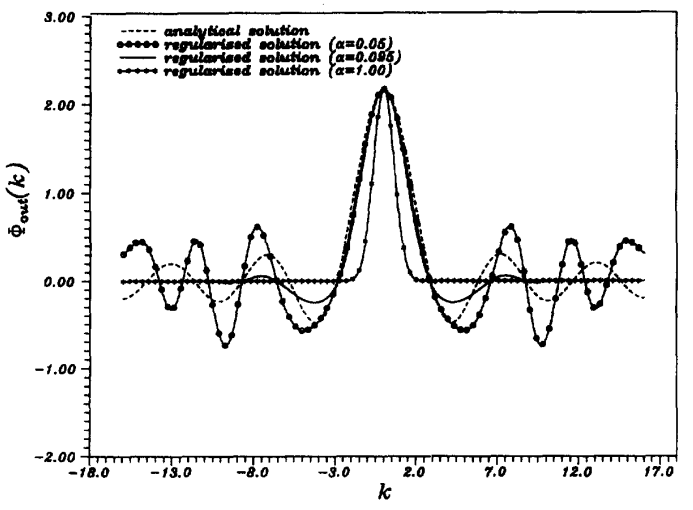

(b) Fourier spectrum of the unknown boundary potential

Fig. 14. The contaminated unknown boundary potentials and their Fourier spectra by using the Gaussian window, $e^{-\alpha k^2}$, with different values of α in the deconvolution analysis for case 1.

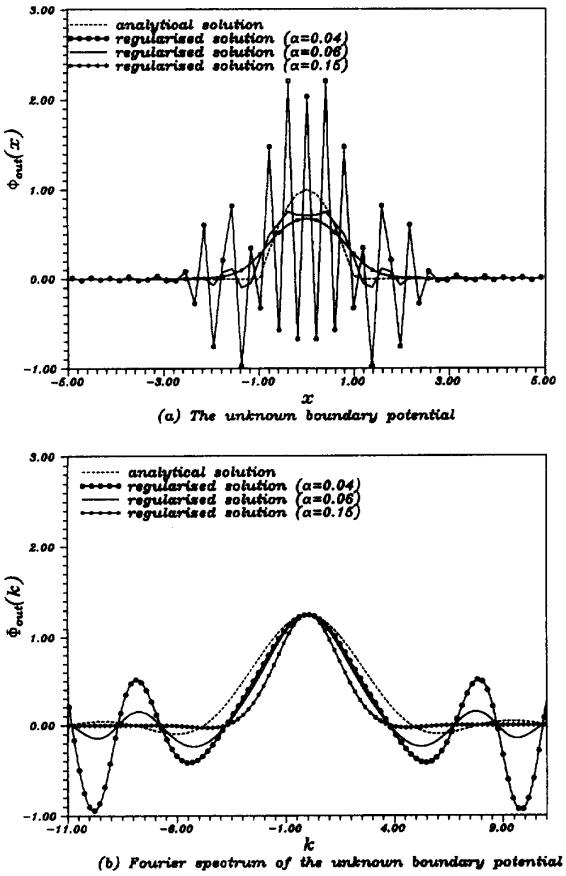

Fig. 15. The contaminated unknown boundary potentials and their Fourier spectra by using the Gaussian window, $e^{-\alpha k^2}$, with different values of α in the deconvolution analysis for case 2.

the corner, the residual norm grows very quickly and deviates very far from the analytical solution. If the value of α is larger than the corner value, then the lower wave-number content will be over-decayed, and the unknown boundary potentials will become smaller. If the corner of the L-curve is chosen as an optimal point, the appropriate value is 0.095 for case 1 and 0.06 for case 2, respectively. The original and regularized amplitudes of the transfer functions are shown in Fig. 18. It can be found that the amplitude of low wave-number for the original transfer function is just slightly reduced by using the $e^{-\alpha k^2}$ window while the amplitude of the high wave-number for the transfer function has been supressed very much. Therefore, the deconvolution result will be regularized to approximate the analytical solution, as shown in Figs. 19 and 20. We can find that the appropriate solutions obtained by using the regularization technique look more reasonable in comparison with the analytical solution than do the results obtained without using regularization. Although some differences still occur between the given curve and reconstruction data, and they can be explained by the discontinuous potential for case 1 and discontinuity of slope in case 2.

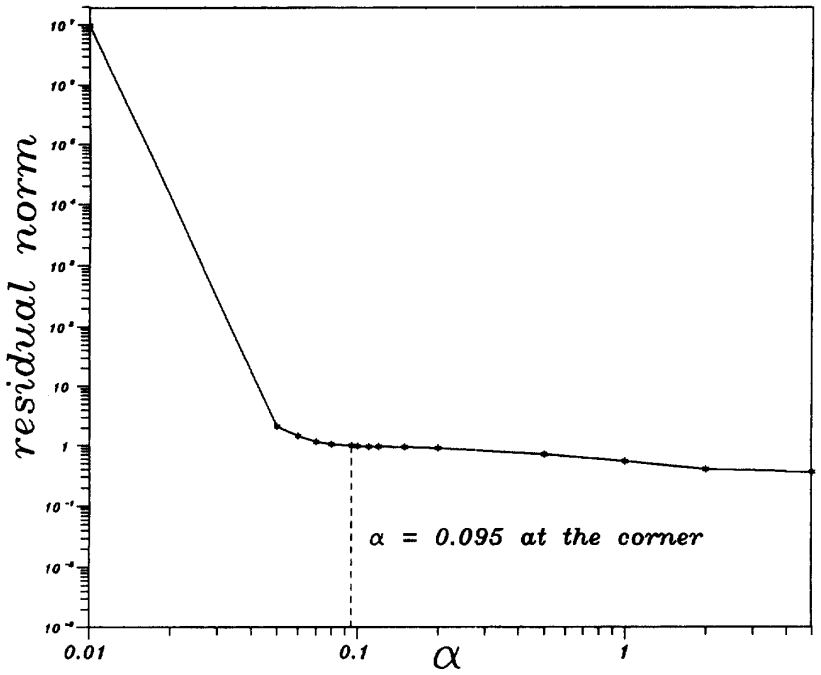

Fig. 16. L-curve in the deconvolution analysis for case 1.

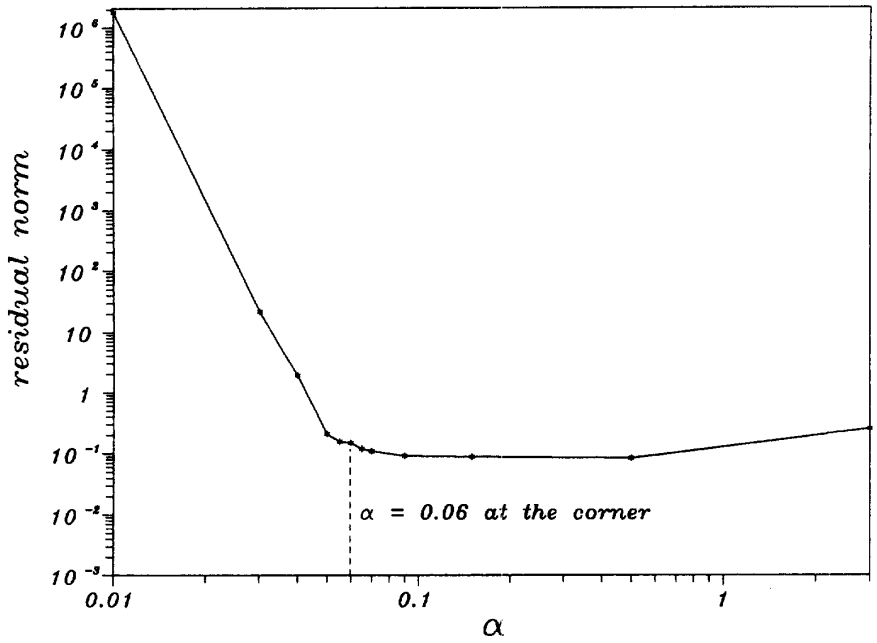

Fig. 17. L-curve in the deconvolution analysis for case 2.

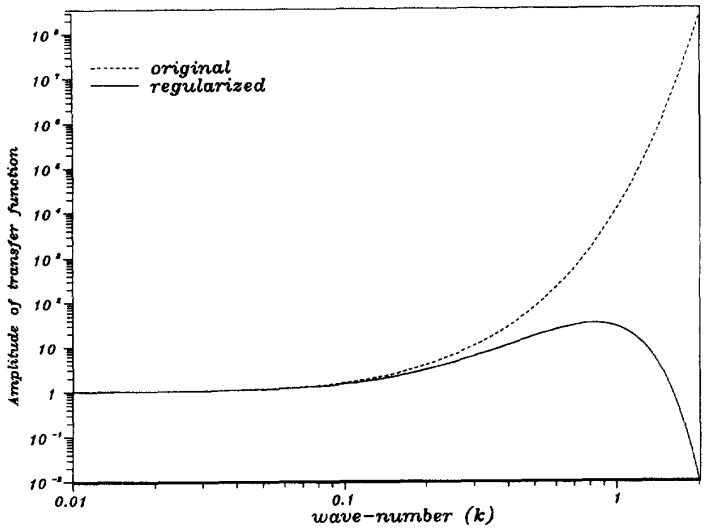

Fig. 18. The original and regularized amplitudes of the transfer function for deconvolution.

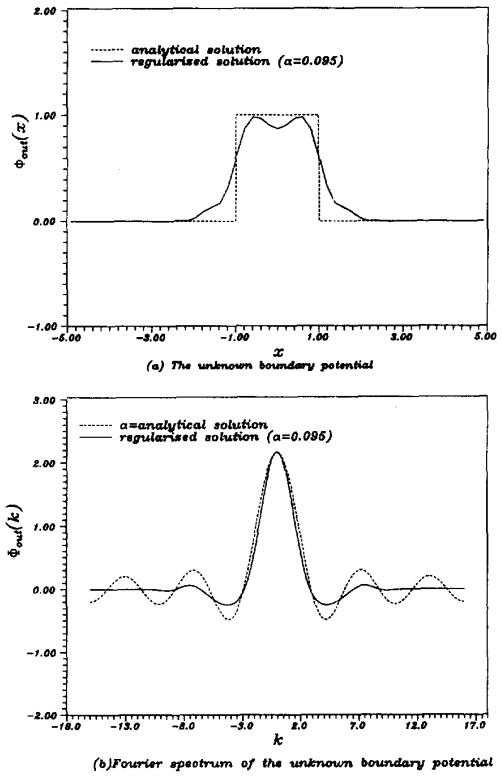

Fig. 19. The contaminated unknown boundary potential and its Fourier spectrum by using the Gaussian window, $e^{-\alpha k^2}$, with the optimal value of α in the deconvolution analysis for case 1.

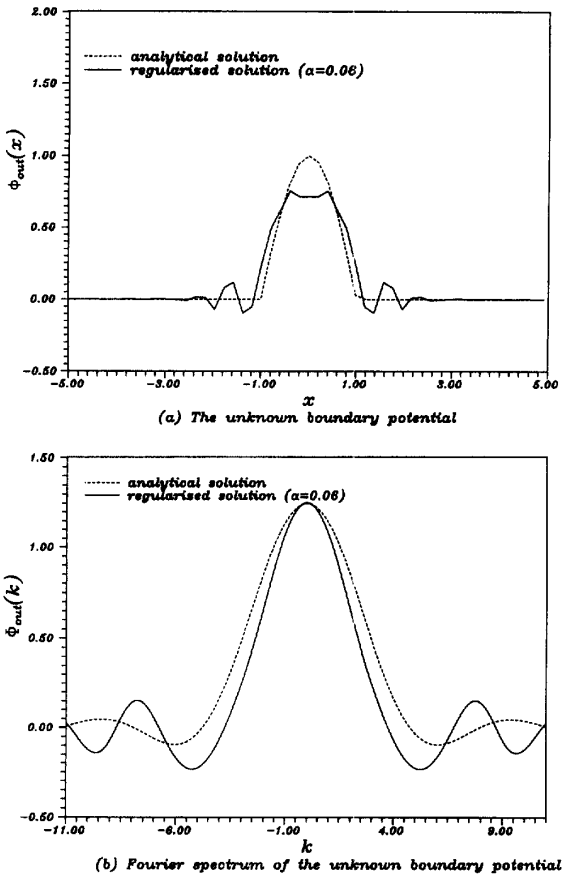

Fig. 20. The contaminated unknown boundary potential and its Fourier spectrum by using the Gaussian window, $e^{-\alpha k^2}$, with the optimal value of α in deconvolution analysis for case 2.

6. Conclusions

The direct and inverse problems can be classified by using the bounded and unbounded transfer functions, respectively. A comparison of the ill-posed problem among the wave equation, Laplace equation and heat conduction equation with overspecified B.C.s is given in Table 1. The regularization technique using the Gaussian window, $e^{-\alpha k^2}$, together with the L-curve, plays a role in determining the optimal parameter α of the window which can maintain the system characteristics and can make the system insensitive to contaminating noise. Therefore, the long standing abstrusity of determining the window by engineering judgement has been solved by using a theoretical window in conjunction with the L-curve. Two examples for the direct and inverse problems, with and without artificial errors, have been given to demonstrate the validity of this proposed method.

Table 1
Comparison of the Laplace equation, wave equation and heat conduction

	Wave equation (soil dynamics)	Laplace equation	Heat conduction
G.E. (original domain)	$\frac{\partial^2 u}{\partial x^2} = \frac{1}{c^2}\frac{\partial^2 u}{\partial t^2}$	$\frac{\partial^2 u}{\partial x^2} + \frac{\partial^2 u}{\partial y^2} = 0$	$\alpha^2 \frac{\partial^2 u}{\partial x^2} = \frac{\partial u}{\partial t}$
Fourier domain	$\frac{\partial^2 U}{\partial x^2} + \frac{\omega^2}{c^2} U = 0$	$\frac{\partial^2 U}{\partial x^2} - k^2 U = 0$	$\frac{\partial^2 U}{\partial x^2} - i\omega U = 0$
Boundary condition	$u(0,t) = a(t),\ \frac{\partial u}{\partial x}(0,t) = 0$	$u(x,0) = \phi(x),\ \frac{\partial u}{\partial y}(x,0) = 0$	$u(0,t) = a(t),\ \frac{\partial u}{\partial x}(0,t) = 0$
Transfer function (direct problem)	$H(\omega) = \frac{1}{\cos\left(\frac{\omega l}{c\sqrt{1+2\xi i}}\right)}$	$H(k) = \frac{1}{\cosh(kl)}$	$H(\omega) = \frac{1}{\cosh\left(\frac{\sqrt{\omega i}\, l}{\alpha}\right)}$
Transfer function (inverse problem)	$H(\omega) = \cos\left(\frac{\omega l}{c\sqrt{1+2\xi i}}\right)$	$H(k) = \cosh(kl)$	$H(\omega) = \cosh\left(\frac{\sqrt{\omega i}\, l}{\alpha}\right)$
Order of infinity	$\frac{1}{2} e^{(l\xi/c)\omega}$	$\frac{1}{2} e^{kl}$	$e^{(\sqrt{\omega}/\sqrt{2\alpha})l}$
Index of ill-posedness	$\frac{l\xi}{c}\omega$	kl	$\frac{\sqrt{\omega}}{\sqrt{2\alpha}} l$

Notations

α	parameter of window function, $e^{-\alpha k^2}$
k	wave-number in the Fourier domain
N	total number in the Fourier transform
k_n	nth wave-number in the Fourier transform
(x,y)	position vector
l	thickness of the strip
$T^{\phi}_{d_1}(k,y), T^{\varphi}_{d_1}(k,y)$	transfer functions of direct problems in the k domain for model 1
$T^{\phi}_{d_2}(k,y), T^{\varphi}_{d_2}(k,y)$	transfer functions of direct problems in the k domain for model 2
$T^{\phi}_{i_1}(k,y), T^{\varphi}_{i_1}(k,y)$	transfer functions of inverse problems in the k domain for model 1
$T^{\phi}_{i_2}(k,y), T^{\varphi}_{i_2}(k,y)$	transfer functions of inverse problems in the k domain for model 2
$\phi_{\text{in}}(x)$	known boundary potential in the x domain
$\Phi_{\text{in}}(k)$	known boundary potential in the k domain
$\varphi_{\text{in}}(x)$	known boundary flux in the x domain
$\Psi_{\text{in}}(k)$	known boundary flux in the k domain
$W_\alpha(x)$	reproducing kernel

Acknowledgements

The authors are grateful to Dr. David Yeih for valuable discussion.

References

[1] D. Yieh, Inverse problems in elasticity, Ph.D. Dissertation, Northwestern University, 1991.
[2] M. Tanaka, H.D. Bui (Eds.), Inverse Problems in Engineering Mechanics, IUTAM symposium, Springer, Berlin, 1992.
[3] V.K. Ivanov, The Cauchy problem for Laplace equation in an infinite strip, Differentsial'nye Uravneniya 1 (1965) 131–136.
[4] L.Y. Chen, J.T. Chen, H.-K. Hong, C.H. Chen, Application of Cesàro mean and the L-curve for the deconvolution problem, Soil Dynamics Earthquake Engineering 14 (1995) 361–373.
[5] P.B. Schnabel, J. Lysmer, H.B. Seed, SHAKE – A computer program for earthquake response analysis of horizontally layered sites. EERC report 72/12, University of California, 1972.
[6] W.J. Silva, Soil response to earthquake ground motion, EPRI Report NP-5747, Electric Power Research Institute, Palo Alto, California, 1988.
[7] H.-K. Hong, J.T. Chen, On the dual integral representation and its application to vibration problems, in: C.A. Brebbia, J.J. Rencis (Eds.), Proceeding 15th International Conference on BEM in Engineering, Worester, Massachusetts, 1993, pp. 377–392.
[8] J.T. Chen, H.-K. Hong, On the relations of hypersingular kernel and divergent series in heat conduction problem using BEM, in: H. Pina, C.A. Brebbia (Eds.), Boundary Element Technology VIII, Computational Mechanics Publication, Southampton, 1993, pp. 115–124.
[9] C.S. Yeh, H.-K. Hong, J.T. Chen, The application of dual integral representation on the shear beam subjected to random excitations, Proceeding of the 16th National Conference on Theoretical and Applied Mechanics, Keelung, Taiwan (in Chinese), 1992, pp. 767–774.
[10] J.T. Chen, H.-K. Hong, C.S. Yeh, S.W. Chyuan, Integral representations and regularizations for divergent series solution of a beam subjected to support motions, Earthquake Engineering and Structural Dynamics 25(9) (1996) 909–925.
[11] J.T. Chen, Y.S. Cheng, Dual series representation for a string Subjected to Support Motions, Advances in Engineering Software 27(3) (1996) 227–238.
[12] J.T. Chen, On a dual integral representation and its applications to computational mechanics, Ph.D. Dissertation, Department of Civil Engineering, National Taiwan University, 1994.
[13] J.T. Chen, D.H. Tsaur and H.-K. Hong, A alternative method for transient and random responses subjected to support motions, Engineering Structures 19(2) (1997) 162–172.
[14] P.C. Hansen, Analysis of discrete ill-posed problems by means of the L-curve, SIAM Review 34 (4) (1992) 561–580.